Parameter estimation of correlated photon pairs

Internship report

submitted by

Jan Gößwein

Registration number 212968

Supervisors:	Prof. Dr. Thomas Pertsch
	Dr. Frank Setzpfandt
	M.Sc. Masoud Safari Arabi
Institute:	Insitute of Applied Physics

Table of Contents

Glossary

Abbreviation	Description	Page
BBO	beta-barium borate	2, 10
BPM	birefringent phase matching	2
CAR	coincidence-to-accidentals ratio	11
KTP	potassium titanyl phosphate	2
LN	lithium niobate	2
mmBE	multi-mode Bose-Einstein	8, 9, 13, 14, 23
QPM	quasi phase matching	2
SPDC	spontaneous parametric down-conversion	1–3, 5, 8–10

List of Figures

List of Tables

1. Introduction

In recent years, quantum technologies have influenced several fields, including communication, computing, sensing, and imaging. They all have one thing in common: they utilize the non-classical properties of light to improve state-of-the-art technology beyond its existing limits.
Specifically, in quantum imaging and sensing, the quantum nature of light is exploited, so light is considered not only as electromagnetic waves, but also as single photons.
In classical imaging, system parameters like spatial resolution or sensitivity are constrained by the diffraction and shot noise limit. Quantum imaging aims to address some of these constraints by making use of quantum properties of light such as entanglement, photon-number correlations, and squeezing [3, 18].
Among the available quantum light sources, spontaneous parametric down-conversion (SPDC) is widely used to generate photon pairs that are correlated in various degrees of freedom, including time, space, and polarization [18].
One example of an imaging technique that uses spatially correlated photons is Quantum ghost imaging. In this technique, an image of an object is reconstructed by measuring the intensity correlations between two spatially separated light beams produced by SPDC. One beam interacts with the sample but is detected with a bucket detector while no spatial information is recorded. The other beam, which does not interact with the sample, is measured with a spatially resolving detector. The spatial information of the sample is recovered by considering the spatial correlation between the two beams [7, 16].
Another imaging technique uses time correlation of the photon pairs. These photons are particularly important in detection schemes based on coincidence measurements. One photon of the pair is sent through a sample while the other is detected directly. Coincidence measurements between the two detection events can then identify photons that were truly part of a pair. This suppresses uncorrelated background noise [18]. This approach will be referred to as the coincidence approach in the following. It will be compared with the scenario in which only one photon of the pair is sent through the sample, with the second photon being neglected. Since this represents a classical transmission experiment, it will be referred to as the conventional approach. It has been shown that the coincidence approach has advantages in terms of precision over the conventional one [19, 20].
For certain biological samples, such as living cells, it is necessary that the wavelength of photons is in the mid-infrared (MIR) to ensure a non-destructive interaction with the sample. This wavelength range corresponds to fundamental vibrational absorption bands [10, 11]. However, a major technical challenge in the MIR regime is the low detection efficiency of the detectors and hence a high level of noise. In particular, thermal background radiation leads to high dark count rates and a low signal-to-noise ratio [22].
As mentioned above, it has been shown that in the absence of noise and with an efficient setup using coincidence measurements offers an advantage compared to conventional meth-

ods. This work aims to determine if measurements using temporally correlated photon pairs still offer advantages over conventional single-photon experiments in regimes of large noise. First, the mechanism behind producing correlated photon pairs is explained. Then, a procedure for modeling the precision of the parameter estimation is introduced for both the correlation-based and conventional approaches. Next, the photon statistics are explained, as well as the setup used to verify those statistics experimentally. Furthermore, the experimental results are compared with the theoretical predictions. Finally, different parameter regions are simulated in order to find combinations for which the correlation-based approach is superior using the experimental results.

2. Theory

2.1. Spontaneous parametric down-conversion

To exploit the advantages of quantum imaging and sensing, one needs to create correlated biphoton states of light. One approach to create such quantum states are sources using spontaneous parametric down-conversion (SPDC). The underlying process is as follows: an incident pump photon with frequency ω_p causes a nonlinear material response resulting in the spontaneous emission of a photon pair with lower frequencies ω_s and ω_i. The subscripts s and i represent the signal and idler photons, as they are usually referred to.
To achieve efficient SPDC processes, the energy and momentum must be conserved. This means that the photon pair must interfere constructively and fulfill the phase-matching conditions [7] :

$$\begin{aligned} \omega_\mathrm{p} &= \omega_\mathrm{s} + \omega_\mathrm{i} \\ \vec{k}_\mathrm{p} &= \vec{k}_\mathrm{s} + \vec{k}_\mathrm{i} - \Delta\vec{k} \end{aligned} \tag{2.1}$$

where the indices p, s and i refer to the pump, signal and idler photon. Δk represents the phase mismatch caused by dispersion, which limits the efficiency of the photon pair generation. A visualization of the conservation processes is shown in Figure 1.
Most experiments use crystals, such as potassium titanyl phosphate (KTP) and beta-barium borate (BBO), or waveguides like lithium niobate (LN), because they exhibit second-order nonlinearity [4, 14, 23].
There are two approaches to compensate for the mismatch. One is called quasi phase matching (QPM) and can be achieved in periodically poled crystals, e.g. KTP or LN, where the nonlinear response also changes periodically, which compensates the mismatch. It allows for a process called type-0 SPDC to happen, which means that all three photons (pump, signal, idler) have the same polarization.
Another way to compensate the mismatch is called birefringent phase matching (BPM) and uses anisotropic materials, such as BBO, as the refractive index changes with the polarization of the incident photon. The effect of using BPM is that the extraordinary photon is

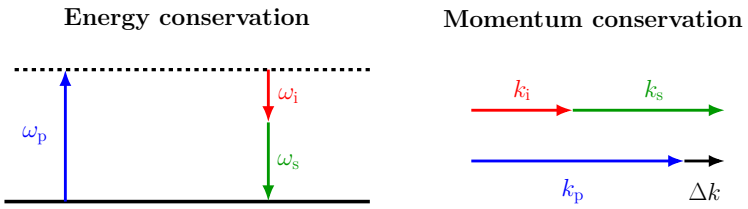

Figure 1.: Conservation processes of collinear SPDC

always polarized perpendicular to the pump. Therefore, no type-0 SPDC can be achieved with this approach. The two other possible cases are called type-I and type-II SPDC. In type-I SPDC the signal and idler photons share the same polarization and are polarized perpendicular to the pump, while in type-II SPDC the signal and idler photons are polarized perpendicular to each other [2].

In this work, the temporal correlation between the signal and idler photons is most commonly used for coincidence measurements. A tool for visualizing the coincidences is a coincidence histogram. These histograms show the number of coincident events as a function of the delay between the arrival times of the photons at two single-photon detectors.

Ideally, the temporal correlation of the photon pairs results in a distinct coincidence peak centered at zero delay if both detectors are the same distance from the SPDC source. The width of this peak depends on several factors, including the resolution of the time-tagging electronics that create a timestamp for each detection event and also on the properties of the generated photon pair.

These correlations are evaluated by defining a temporal interval around the detection peak. Within this interval, detection events are considered true coincidences, meaning they originate from the same source. This interval is usually referred to as the coincidence window τ_{cw}. Events that fall outside this window are usually attributed to uncorrelated background noise and are called accidental counts. A representative scheme of a coincidence histogram is shown in Figure 2 .

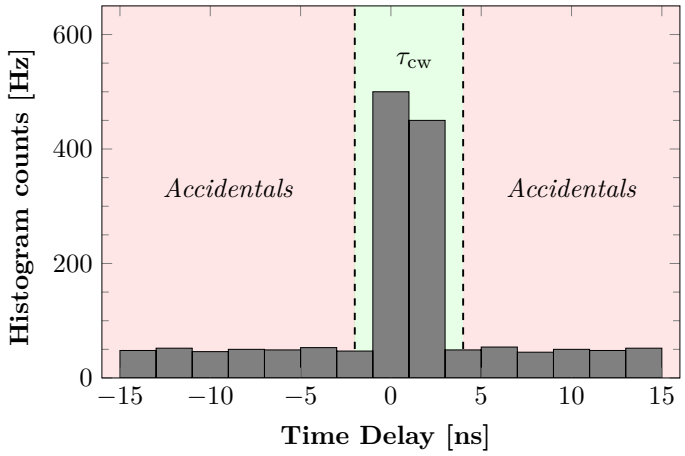

Figure 2.: Schematic of a coincidence histogram

2.2. Model for transmittance estimation

When noise is present in the experimental setup, the question arises as to how precisely the parameters of interest can be determined using either the conventional or coincidence approach. As the objective of this work is to compare both methods in terms of the precision of the measurement rather than focusing on the estimated absolute values, it is the variance of the chosen parameter that is decisive. Since the results of this study will be applied in a transmission setup, the transmittance of the sample is chosen as the key parameter.
In the following, the formulas to calculate the variance of the transmittance are derived both for the conventional and coincidence approach. The arm in which the sample is placed will be referred to as idler and the other arm, the reference arm, as signal. The case in which a sample is placed in the idler arm is denoted with the superscript 'sam', where there is no sample with 'ref'.
Starting with the conventional approach, only the idler arm is required. Therefore, in absence of the sample, the number of total detected counts in this arm is:

$$N_{\mathrm{tot}}^{\mathrm{ref}} = \eta_{\mathrm{idl}}\, N_{\mathrm{g}} + N_{\mathrm{noise}}^{\mathrm{ref}} \tag{2.2}$$

where $N_{\mathrm{tot}}^{\mathrm{ref}}$ is the total number of counts without a sample, η_{idl} is the efficiency of the idler arm, N_{g} is the number of generated photon pairs and $N_{\mathrm{noise}}^{\mathrm{ref}}$ is the number of counts when there are no photon pairs, which refer to noise consisting of e.g. dark counts of the detector or stray light.
When a sample is placed in the idler arm, the total number of counts changes according to the transmittance of the material. Therefore, Equation 2.2 is modified as follows:

$$N_{\mathrm{tot}}^{\mathrm{sam}} = T\, \eta_{\mathrm{idl}}\, N_{\mathrm{g}} + N_{\mathrm{noise}}^{\mathrm{sam}} \tag{2.3}$$

where $N_{\mathrm{tot}}^{\mathrm{sam}}$ represents the total counts in presence of a sample and T is the transmittance of the sample.
T can be calculated combining equations 2.2 and 2.3:

$$T = \frac{N_{\mathrm{tot}}^{\mathrm{sam}} - N_{\mathrm{noise}}^{\mathrm{sam}}}{N_{\mathrm{tot}}^{\mathrm{ref}} - N_{\mathrm{noise}}^{\mathrm{ref}}} \tag{2.4}$$

As can be seen from the formula, four independent measurements must be conducted to retrieve the transmittance: two where only the dark counts are measured with and without the sample, and two with an active laser also with and without the sample.

Based on Equation 2.4 and error propagation, the variance of the transmittance $\mathrm{Var}(T)$ can be calculated assuming that all four variables are independent of each other [13]:

$$\begin{aligned}\mathrm{Var}(T) &= \sum_i \left(\frac{\partial T}{\partial X_i}\right)^2 \mathrm{Var}(X_i) \\ &= \left(\frac{\partial T}{\partial N^{\mathrm{sam}}_{\mathrm{tot}}}\right)^2 \mathrm{Var}(N^{\mathrm{sam}}_{\mathrm{tot}}) + \left(\frac{\partial T}{\partial N^{\mathrm{sam}}_{\mathrm{noise}}}\right)^2 \mathrm{Var}(N^{\mathrm{sam}}_{\mathrm{noise}}) \\ &\quad + \left(\frac{\partial T}{\partial N^{\mathrm{ref}}_{\mathrm{tot}}}\right)^2 \mathrm{Var}\left(N^{\mathrm{ref}}_{\mathrm{tot}}\right) + \left(\frac{\partial T}{\partial N^{\mathrm{ref}}_{\mathrm{noise}}}\right)^2 \mathrm{Var}\left(N^{\mathrm{ref}}_{\mathrm{noise}}\right)\end{aligned} \tag{2.5}$$

When the partial derivatives are explicitly calculated using Equation 2.4 the final formula for the variance of the transmittance is:

$$\mathrm{Var}(T) = \left(\frac{1}{\eta_{\mathrm{idl}}\, N_{\mathrm{g}}}\right)^2 \left[\mathrm{Var}(N^{\mathrm{sam}}_{\mathrm{tot}}) + \mathrm{Var}(N^{\mathrm{sam}}_{\mathrm{noise}}) + T^2\left[\,\mathrm{Var}\left(N^{\mathrm{ref}}_{\mathrm{tot}}\right) + \mathrm{Var}\left(N^{\mathrm{ref}}_{\mathrm{noise}}\right)\,\right]\right] \tag{2.6}$$

When using the coincidence approach, the formulas for the transmittance and it's variance differ. In addition to the idler arm, the signal arm is required to detect correlated photons created by SPDC. Assuming perfectly correlated photon pairs, the formula for pure coincidence counts with and without a sample in the idler arm is as follows [8]:

$$\begin{aligned}N^{\mathrm{sam}}_{\mathrm{cc,pure}} &= T\,\eta_{\mathrm{idl}}\,\eta_{\mathrm{sig}}\,N_{\mathrm{g}} \\ N^{\mathrm{ref}}_{\mathrm{cc,pure}} &= \eta_{\mathrm{idl}}\,\eta_{\mathrm{sig}}\,N_{\mathrm{g}}\end{aligned} \tag{2.7}$$

where $\eta_{\mathrm{sig/idl}}$ is the efficiency of signal and idler arm, T is the transmittance of the sample and N_{g} is the number of generated photon pairs.

In the context of coincidence measurements, it is important to note that the detection of pure coincidences is not the only outcome of such measurements. In addition to these, what is called accidental counts are also detected. Consequently, instead of both photons originating from one pair being detected simultaneously, only one is detected in one arm and a noise photon is detected in the other.Another possibility is that two photons are detected concurrently in both arms, yet neither of them originates from a SPDC-pair. In both cases, the time tagging unit recognizes them as coincidence events. Hence, they are designated as accidental counts.

The following formula is used to model the accidental counts with sample ($R^{\mathrm{sam}}_{\mathrm{ac}}$) and without $\left(R^{\mathrm{ref}}_{\mathrm{ac}}\right)$ [8]:

$$\begin{aligned}R^{\mathrm{sam}}_{\mathrm{ac}} &= \left(T\,\eta_{\mathrm{idl}}R_{\mathrm{g}} + R_{\mathrm{dc,idl}} - R^{\mathrm{sam}}_{\mathrm{cc,pure}}\right)\left(\eta_{\mathrm{sig}}R_{\mathrm{g}} + R_{\mathrm{dc,sig}} - R^{\mathrm{sam}}_{\mathrm{cc,pure}}\right)\tau_{\mathrm{cw}} \\ R^{\mathrm{ref}}_{\mathrm{ac}} &= \left(\eta_{\mathrm{idl}}R_{\mathrm{g}} + R_{\mathrm{dc,idl}} - R^{\mathrm{ref}}_{\mathrm{cc,pure}}\right)\left(\eta_{\mathrm{sig}}R_{\mathrm{g}} + R_{\mathrm{dc,sig}} - R^{\mathrm{ref}}_{\mathrm{cc,pure}}\right)\tau_{\mathrm{cw}}\end{aligned} \tag{2.8}$$

where the variable R denotes the rate of the respective parameters. The total number can be calculated by multiplying the rate by the exposure time. When the exposure time is set to one second, the rate and the total number coincide. $R_{\mathrm{dc,idl/sig}}$ denotes the dark count rate in the idler/signal arm and τ_{cw} is the coincidence window.
Therefore, the measured total coincidence events are the sum of pure and accidental coincidence events:

$$\begin{aligned} N^{\mathrm{sam}}_{\mathrm{cc,tot}} &= N^{\mathrm{sam}}_{\mathrm{cc,pure}} + N^{\mathrm{sam}}_{\mathrm{ac}} \\ N^{\mathrm{ref}}_{\mathrm{cc,tot}} &= N^{\mathrm{ref}}_{\mathrm{cc,pure}} + N^{\mathrm{ref}}_{\mathrm{ac}} \end{aligned} \tag{2.9}$$

Using equations 2.7, 2.8 and 2.9, the transmittance T in the coincidence approach can be obtained as follows:

$$T = \frac{N^{\mathrm{sam}}_{\mathrm{cc,tot}} - N^{\mathrm{sam}}_{\mathrm{ac}}}{N^{\mathrm{ref}}_{\mathrm{cc,tot}} - N^{\mathrm{ref}}_{\mathrm{ac}}} \tag{2.10}$$

In comparison to the conventional approach from Equation 2.4, which necessitates four independent measurements, this approach requires only two: one with and one without the sample. This is due to the fact that accidentals and coincidences can be obtained within a single measurement.
Since the objective is to compare the precision of the transmittance T using the two different approaches, analogue to Equation 2.5, variance of the transmittance can be calculated using error propagation and coincidence counts:

$$\begin{aligned} \mathrm{Var}(T) &= \sum_i \left(\frac{\partial T}{\partial X_i}\right)^2 \mathrm{Var}(X_i) \\ &= \left(\frac{\partial T}{\partial N^{\mathrm{sam}}_{\mathrm{cc,tot}}}\right)^2 \mathrm{Var}\left(N^{\mathrm{sam}}_{\mathrm{cc,tot}}\right) + \left(\frac{\partial T}{\partial N^{\mathrm{sam}}_{\mathrm{ac}}}\right)^2 \mathrm{Var}(N^{\mathrm{sam}}_{\mathrm{ac}}) \\ &\quad + \left(\frac{\partial T}{\partial N^{\mathrm{ref}}_{\mathrm{cc,tot}}}\right)^2 \mathrm{Var}\left(N^{\mathrm{ref}}_{\mathrm{cc,tot}}\right) + \left(\frac{\partial T}{\partial N^{\mathrm{ref}}_{\mathrm{ac}}}\right)^2 \mathrm{Var}\left(N^{\mathrm{ref}}_{\mathrm{ac}}\right) \end{aligned} \tag{2.11}$$

Using equations 2.7 and 2.9, an explicit expression for variance of the transmittance can be obtained:

$$\mathrm{Var}(T) = \left(\frac{1}{\eta_{\mathrm{sig}}\,\eta_{\mathrm{idl}}\,N_{\mathrm{g}}}\right)^2 \left[\mathrm{Var}\left(N^{\mathrm{sam}}_{\mathrm{cc,tot}}\right) + \mathrm{Var}(N^{\mathrm{sam}}_{\mathrm{ac}}) + T^2\left[\mathrm{Var}\left(N^{\mathrm{ref}}_{\mathrm{cc,tot}}\right) + \mathrm{Var}\left(N^{\mathrm{ref}}_{\mathrm{ac}}\right)\right]\right] \tag{2.12}$$

The objective of this work is to ascertain parameter configurations in which the coincidence approach exhibits superiority in terms of precision, as measured by the magnitude of variance of the transmittance, in comparison to the conventional approach. In order to model both variance formulas properly, it is necessary to experimentally investigate the statistics of each parameter of which the variance is calculated.

2.3. Photon statistics

When investigating the statistical properties of photons, it is essential to recognize that different types of light sources exhibit distinct statistical distributions. These distributions are typically characterized by their respective variances, which serve as key indicators of the underlying photon statistics. A coherent laser source is often used as the reference standard, as it represents the most stable form of light emission within the picture of classical optics [6]. In the following, two types of light sources with fundamentally different statistical distributions are examined in greater detail, namely coherent and thermal sources.

2.3.1. Coherent light

From a classical perspective, a coherent light field, such as that produced by a stable laser, may be regarded as a monochromatic electromagnetic wave with well-defined amplitude and phase.
When considering a light beam of constant power P, the photon flux is uniform in time. To describe the detection statistics, the observation time interval T may be subdivided into a large number of subintervals of duration Δt. For each subinterval, the probability of detecting a single photon is small but finite. The probability of detecting two or more photons within a single subinterval can be neglected.
Since the intensity of the beam is constant, the detection probability is identical for each subinterval, and successive detection events are statistically independent.
The probability of detecting n photons within N subintervals of the total observation time T corresponds to the case where n subintervals each contain exactly one photon, while the remaining $(N-n)$ subintervals contain none. This situation is described by the binomial distribution [6]:

$$\mathcal{P}(n) = \frac{N!}{n!\,(N-n)!}\, p^n (1-p)^{N-n} \tag{2.13}$$

where p denotes the probability of detecting a photon in a single subinterval. This probability is equal to the average number of detected photons $\langle n \rangle$ in the observation interval divided by the number of subintervals N:

$$p = \frac{\langle n \rangle}{N} \tag{2.14}$$

Substituting this expression into Equation 2.13 yields:

$$\mathcal{P}(n) = \frac{N!}{n!\,(N-n)!} \left(\frac{\langle n \rangle}{N}\right)^n \left(1 - \frac{\langle n \rangle}{N}\right)^{N-n} \tag{2.15}$$

In the limit $N \to \infty$, it can be shown [6] that the probability of detecting n photons in a coherent light beam reduces to:

$$\mathcal{P}(n) = \frac{\langle n \rangle^{\,n}}{n!}\, e^{-\langle n \rangle} \tag{2.16}$$

This result corresponds to a **Poisson distribution**, which is characteristic for coherent light sources. A distinctive property of the Poisson distribution is that the mean photon number $\langle n \rangle$ is equal to its variance, i.e. $\langle n \rangle = \mathrm{Var}(n)$.
Furthermore, it has been demonstrated that the coincidence counts of photon pairs generated via SPDC also follow a Poissonian distribution, since the SPDC process preserves the coherence of the incident pump laser [1, 12, 21]. Consequently, the variance of the coincidence counts in Equation 2.12 can likewise be approximated by their mean value, $\mathrm{Var}(N_{\mathrm{cc,tot}}) \approx \langle N_{\mathrm{cc,tot}} \rangle$.

2.3.2. Thermal light

In contrast to coherent light sources, which exhibit Poissonian photon statistics, thermal light displays fundamentally different statistical properties. Thermal radiation arises from the random emission of photons in a hot body, where the optical field consists of a large number of independently oscillating modes. Each mode can occupy quantized energy levels depending on their angular frequency ω:

$$E_n = \left(n + \tfrac{1}{2}\right)\hbar\omega, \qquad n \geq 0, \tag{2.17}$$

where n denotes the photon number.
Using the quantization of energy levels and Planck's law, the probability of finding n photons in a single mode is then governed by Boltzmann's law:

$$\mathcal{P}_\omega(n) = \frac{\exp(-n\hbar\omega/k_B T)}{\sum_{m=0}^{\infty} \exp(-m\hbar\omega/k_B T)} \tag{2.18}$$

It can be shown that the mean photon number $\langle n \rangle$ can be expressed as:

$$\langle n \rangle = \frac{1}{\exp(\hbar\omega/k_B T) - 1} \tag{2.19}$$

Substituting this expression into Equation 2.18, the probability distribution can be rewritten as follows:

$$\mathcal{P}_\omega(n) = \frac{1}{\langle n \rangle + 1} \left(\frac{\langle n \rangle}{\langle n \rangle + 1}\right)^n \tag{2.20}$$

This distribution is referred to as single-mode **Bose-Einstein distribution** [6].
In practice, thermal light sources generally populate a large number of independent modes. Consequently, the multi-mode expansion of the Bose-Einstein distribution must be considered. Assuming that m modes of the field are occupied and that the thermal light is fully unpolarized, the multi-mode Bose-Einstein (mmBE) distribution can be expressed as [17]:

$$\mathcal{P}_m(n) = \frac{(n+m-1)!}{(m-1)!\,n!} \frac{\langle n \rangle^n}{(1 + \langle n \rangle/m)^m \, (\langle n \rangle + m)^n} \tag{2.21}$$

The combinatorial prefactor accounts for the number of ways in which n photons can be distributed among m modes, while the remaining factor describes the joint probability associated with the m occupied modes. As a consistency check, it is readily verified that for $m = 1$ the expression reduces to the single-mode Bose-Einstein distribution given in Equation 2.20.

The variance of the photon number in the mmBE distribution is given by:

$$\mathrm{Var}(n) = \langle n \rangle \left(1 + \frac{\langle n \rangle}{m}\right) \tag{2.22}$$

When compared to the variance of a Poissonian distribution, which is equal to its mean value, it is evident that the mmBE distribution always exhibits larger fluctuations. Hence, thermal light is intrinsically super-Poissonian. This property is commonly described in terms of photon bunching, meaning that photons tend to arrive in groups more frequently than would be expected for the random distribution characteristic of coherent (Poissonian) light. From this perspective, coherent sources represent the most stable classical form of light in terms of intensity, while any source with time-dependent fluctuations, such as thermal radiation, necessarily shows enhanced photon-number fluctuations and thus super-Poissonian statistics.

In the limit $m \to \infty$, the variance of the mmBE distribution approaches the Poissonian result, as can be seen directly from Equation 2.22. This reflects the fact that in the presence of infinitely many modes, the photon statistics become indistinguishable from those of a coherent source.

It was shown that each photon from a SPDC process exhibits mmBE statistics, whether it is a signal or idler photon [12]. The mode number m and, consequently, the variance depend on the chosen setup and must be determined individually.

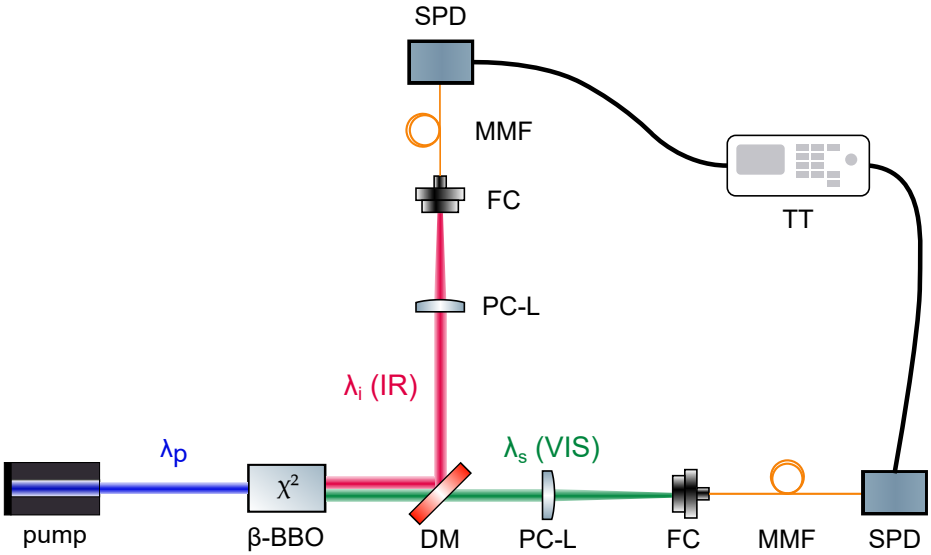

Figure 3.: Experimental setup; DM: dichroic mirror, FC: fiber coupling, MMF: multi-mode fiber, PC-L: plano-convex lens, Sam: sample, SPD: single photon detector, TT: time tagging unit

3. Experimental Setup

To establish a consistent model that predicts conditions in which the coincidence approach shows in more precise results compared to the conventional, the assumptions for the different unknown parameters (e.g., the variance of coincidence and accidental counts) must align with the results obtained in an experimental setup. Therefore, the following section explains the setup used to measure the photon statistics in more detail.

A sketch of the setup is shown in Figure 3. It consists of a BBO crystal that produces temporally correlated photon pairs through type-I SPDC. The idler photon lies in the infrared range at a wavelength of $\lambda_i = 1404$ nm, while the signal photon is in the visible spectrum at a wavelength of $\lambda_s = 571$ nm. The crystal is pumped by a diode laser operating at $\lambda_p = 407.7$ nm.

The signal and idler photons are separated by a dichroic mirror. The signal photons are then focused into a fiber coupling device with a plano-convex lens that has a focal length of 30 mm. The same process is used for the idler photons, but the plano-convex lens has a focal length of 15 mm.

Both signal and idler photons are coupled to single photon detectors using multi-mode fibers. Both detectors are connected to a time-tagging unit to obtain the arrival time of the photons in each arm and find the coincidence events.

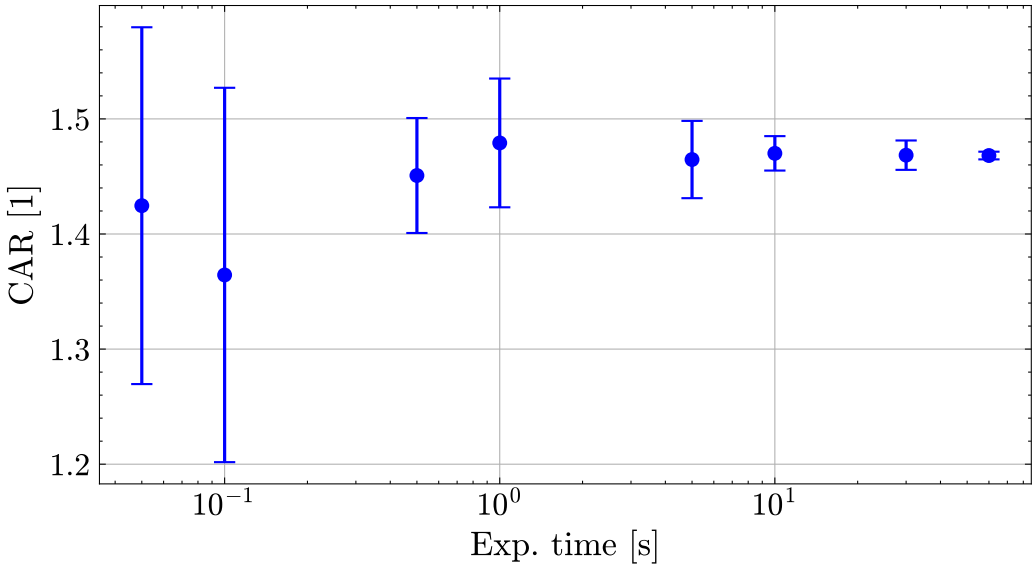

Figure 4.: Coincidence-to-Accidentals ration for different exposure times

4. Results

4.1. Coincidence-to-accidentals ratio

One issue that must be addressed when determining the statistics of the different parameters is that the coincidence-to-accidentals ratio (CAR) depends on the exposure time. Therefore, before measuring the statistical distributions, an exposure time must be found for which the CAR value remains constant. Thus, this value was measured for nine exposure times ranging from ten milliseconds to sixty seconds. The integration time was set to ten times the exposure time for each measurement. Hence, ten histograms were saved for each exposure time and based on these histograms, the average CAR value and its standard deviation were calculated.
The results are shown in Figure 4. As the exposure time increases, it can be seen that the fluctuation of the CAR value, i.e. its standard deviation, decreases. Furthermore, after an exposure time of one second, the CAR value remains approximately constant. Therefore, this range from one second onwards is preferred for statistical analysis. However, as this requires many consecutive and lengthy measurements, the aim is to use the shortest possible exposure time at which the CAR value remains constant. Therefore, one second will be used as the exposure time for upcoming measurements.

4.2. Dark counts

The first parameter to be determined is the statistical distribution of dark counts in both arms. This result is necessary for obtaining the variance of noise in the conventional ap-

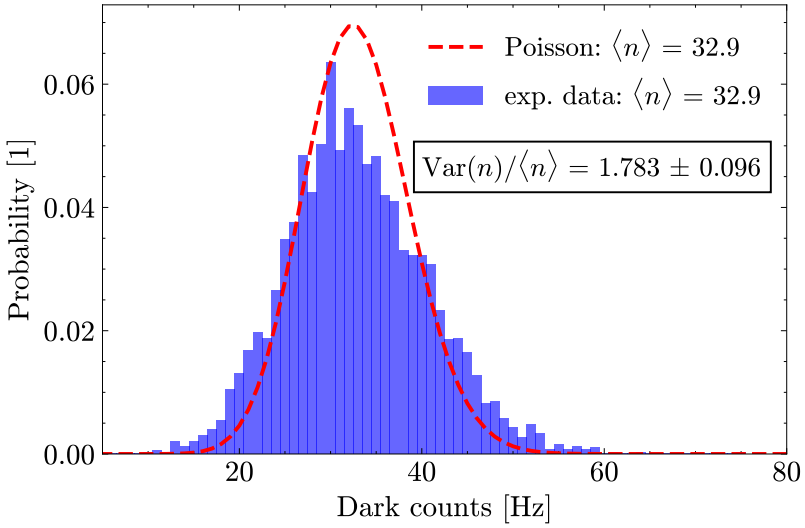

Figure 5.: Dark counts of the IR single photon detector in the idler arm

proach in Equation 2.6. For the measurement, the exposure time was set to one second, and the integration time was set to one thousand seconds. To obtain the intrinsic dark counts, both single-photon detectors were disconnected from the setup and the measurement was repeated five times.

The measurement results for the idler arm can be seen in Figure 5. It shows the probability distribution for each dark count rate. Additionally, a Poisson distribution was fitted to the experimental data with the same average count rate. This was done because it is expected that the dark counts of single-photon detectors will exhibit a Poisson distribution [5]. However, the two distributions do not match, indicating that the experimentally obtained data does not follow a Poisson distribution. This is also confirmed by calculating the variance-to-mean ratio, which, in the case of a Poisson distribution, should equal one. The ratio was calculated for each of the five repeats and averaged to 1.78. This is shown in the black box of Figure 5.

This mismatch may be caused by the afterpulsing effect. This effect refers to spurious detection events that occur shortly after genuine photon detection, even though no new photons have arrived. These false counts arise from trapped charge carriers released after the detector resets, triggering a secondary avalanche. This effect is well-known in InGaAs single-photon detectors operating in the infrared, such as the one used in this experiment [15]. Consequently, this effect can be interpreted as a bunching of detection events and hence those cannot be considered independet anymore. In analogy of the thermal light, this bunching results in a larger variance compared to a Poissonian distribution.

A strong indication that the mismatch is caused by afterpulsing is that the probability of afterpulsing events decreases exponentially with the detector's dead time. Since individual afterpulses could not be measured directly, the variance-to-mean ratio was measured instead. As the number of correlated events decreases as the probability of afterpulsing decreases,

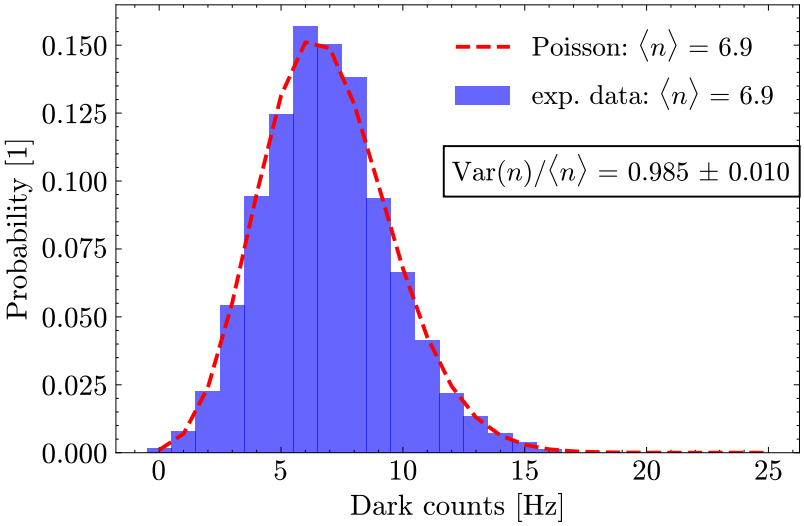

Figure 6.: Dark counts of the VIS single photon detector in the signal arm

the variance-to-mean ratio should also decrease and approach one, as in a Poisson distribution [9]. The exponential decay of the variance-to-mean ratio is shown in the appendix in Figure A.2, thus confirming that the mismatch is caused by afterpulsing.
For the analysis of the dark counts in the signal arm, which are in the visible range, the same experimental settings as for the idler arm were used. The statistical distribution of the dark counts in the signal arm can be seen in Figure 6. As for the idler arm, a Poissonian fit was added to the figure. This shows that the distribution of dark counts matches the Poisson distribution very well. It is confirmed by considering the variance-to-mean ratio of the counts, shown in the black box, which was calculated for each of the five repeats. On average, it yields 0.985, indicating that it can be well approximated by a Poisson distribution.

4.3. Single counts

To correctly model Equation 2.6 and the variance of the total photon counts (i.e.,$\mathrm{Var}\left(N_{\mathrm{tot}}^{\mathrm{ref}}\right)$ and $\mathrm{Var}(N_{\mathrm{tot}}^{\mathrm{sam}})$), the statistics of the idler arm were investigated experimentally.
For the measurement, the exposure time was set to one second and the integration time to one thousand seconds. Thus, each measurement yielded 1,000 data points for statistical analysis. The measurement was repeated five times to account for statistical fluctuations and determine an interval for the variance-to-mean ratio. The results of the measurements are shown in Figure 7.
The average photon number $\langle n \rangle$ is 65,107. Furthermore, the mode number m_{theo}, which was determined using the experimental variance value and Equation 2.22, is 61,384. Based on these two values, a mmBE and a Poisson distribution were modeled. As can be seen, the Poisson distribution significantly overestimates the peak of the experimental distribution. Additionally, the Poisson distribution decreases faster than the experimental distribution,

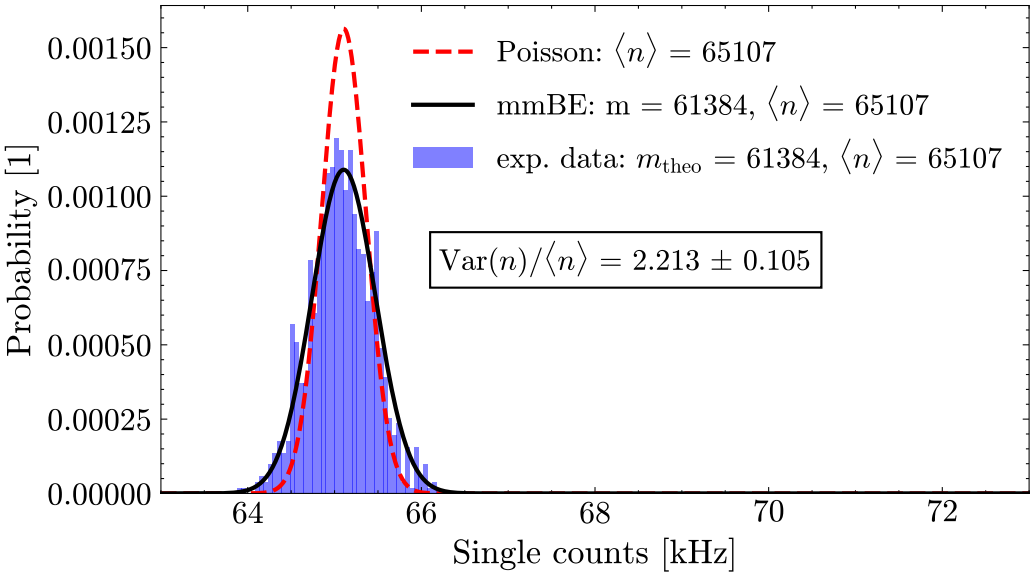

Figure 7.: Photon statistics in the idler arm

so the edges of the distribution are not modeled correctly. On the other hand, the mmBE fit agrees much better with the experimental distribution because it properly estimates the peak and the edges of the experimental distribution fall within the theoretical fit.

The black box shows the variance-to-mean ratio for the five repeated measurements. The mean value is 2.2, with a standard deviation of 0.1. Since this ratio is not equal to one, it confirms that the experimental distribution is not Poisson but has a higher variance. For the modeling of the variance of the single counts, this means that $\mathrm{Var}\left(N_{\mathrm{tot}}^{\mathrm{ref}}\right)$ and $\mathrm{Var}(N_{\mathrm{tot}}^{\mathrm{sam}})$ can be approximated by the mean photon number multiplied with a factor of 2.2.

As a consistency check, the statistics of the photons in the signal arm were also measured, as they should exhibit a mmBE distribution. The experimental parameters are kept the same as in the idler arm measurements.

The results can be seen in Figure 8. The approach for calculating the Poisson and mmBE distribution is the same as for the idler photons. Similar to the idler arm, the mmBE model more closely resembles the experimental distribution than the Poisson model because it overestimates the peak and underestimates the edges of the distribution. This is confirmed once more by calculating the variance-to-mean ratio, which yields an average of 1.9 and shows that the distribution is not Poissonian.

The count rate of the signal photons is roughly 30 times higher than the idler photons. One reason for this may be that the idler photon spectrum is much broader than the signal's. Consequently, the spatial cone of the emitted idler photons is larger. The focusing lens may have a smaller clear aperture than the spatial extent of the cone, resulting in some photons being clipped. Meanwhile, the focusing lens in the signal arm collects the entire spectrum. Another reason may be that, due to the broader spectrum in the idler arm, the chromatic aberration of the lens leads to different focal lengths, so not the entire spectrum is coupled

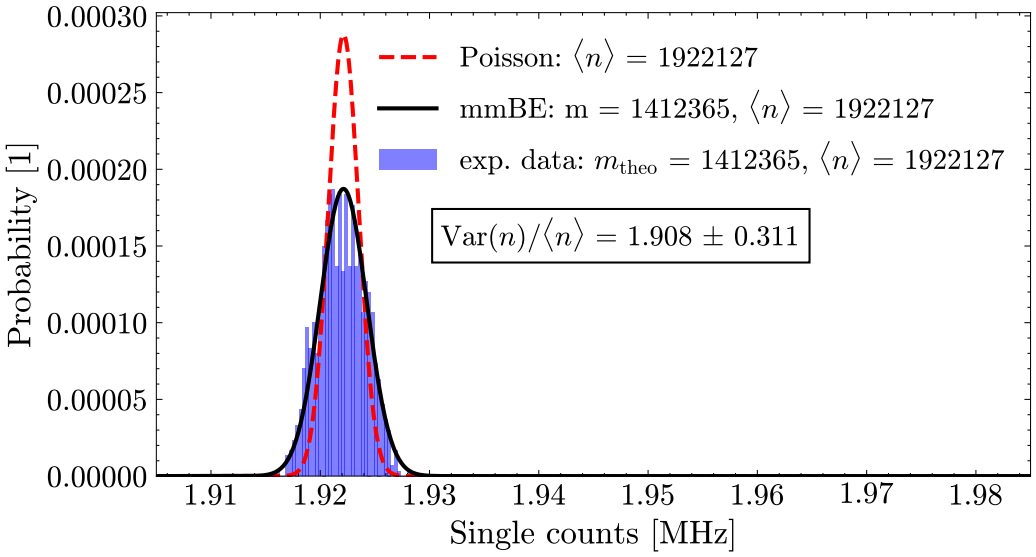

Figure 8.: Photon statistics in the signal arm

into the fiber. Since the mode number (m_{theo}) is directly related to the average photon number, a high count rate also results in a significantly larger mode number.

4.4. Coincidence counts

To determine the statistics of the coincidence counts that are required to calculate the variance of the transmittance in Equation 2.12, five measurements were performed. The experimental parameters were kept the same as in the previous section for the singles. Therefore, an exposure time of one second and an integration time of one thousand seconds was used. For every step in time, a histogram was saved by the time-tagging unit. The bin width was set to 4.68 ns and the number of bins to 200. The coincidence window was set to $\tau_{\text{cw}} = 9.36$ ns, which means that two bins were selected as coincidence counts.
The results of the measurements are shown in Figure 9. Similarly to the single counts, a Poisson distribution is modeled based on the average photon counts observed in the experiment. As can be seen, the experimental distribution is well approximated by the Poisson distribution. This is confirmed by considering the variance-to-mean ratio illustrated in the black box. An average value of 1.040 and a standard deviation of 0.035 are achieved for the five measurements. This coincides with the theoretical prediction in subsubsection 2.3.1 that coincidence counts can be approximated by a Poisson distribution where the variance equals the mean.
Consequently, the variance of the coincidence counts in the model for the simulation can be substituted by the average coincidence counts.

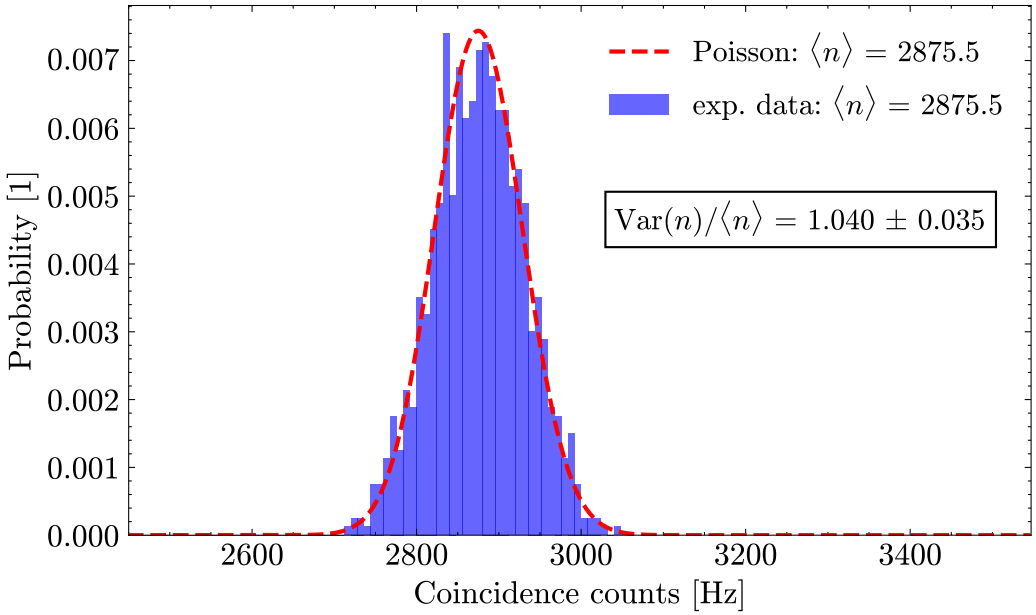

Figure 9.: Photon statistics of coincidence counts

4.5. Accidental counts

Regarding accidental counts, two parameters have to be determined experimentally. Not only must the variance of the accidental counts be measured for Equation 2.12, but also Equation 2.8 for calculating them from single and coincidence counts.

For the variance measurement, the exposure time was set to one second and the integration time to sixty seconds. The histogram of the coincidences was used to retrieve the accidental counts. The bin width was set to 1.4 ns and the number of bins to 110. The coincidence window was set to 2.8 ns, which means that two bins were selected as coincidence counts. A representative histogram can be seen in appendix in Figure A.1.

The statistical distribution is shown in Figure 10. Similar to previous results, a Poisson distribution was modeled based on average accidental counts. As can be seen, the Poissonian fit closely matches the experimental distribution.

To obtain a quantitative measure of the distribution in addition to a qualitative one, the variance-to-mean ratio was again calculated. For each time step, 105 values were obtained for the accidental counts, and the variance-to-mean ratio was determined. Then, the average and standard deviation of the ratio were calculated for the sixty steps. The result is shown in the black box of Figure 10.

Within the limits of the standard deviation, the ratio corresponds to one, which is the ratio of a Poisson distribution. Therefore, the accidental counts can be assumed to have a Poisson distribution, and the variance can be substituted by the average accidental count.

Additionally, it has to be validated if the formula for calculating the accidentals in Equation 2.8 matches the experimental data. For this evaluation, histograms from the statistical

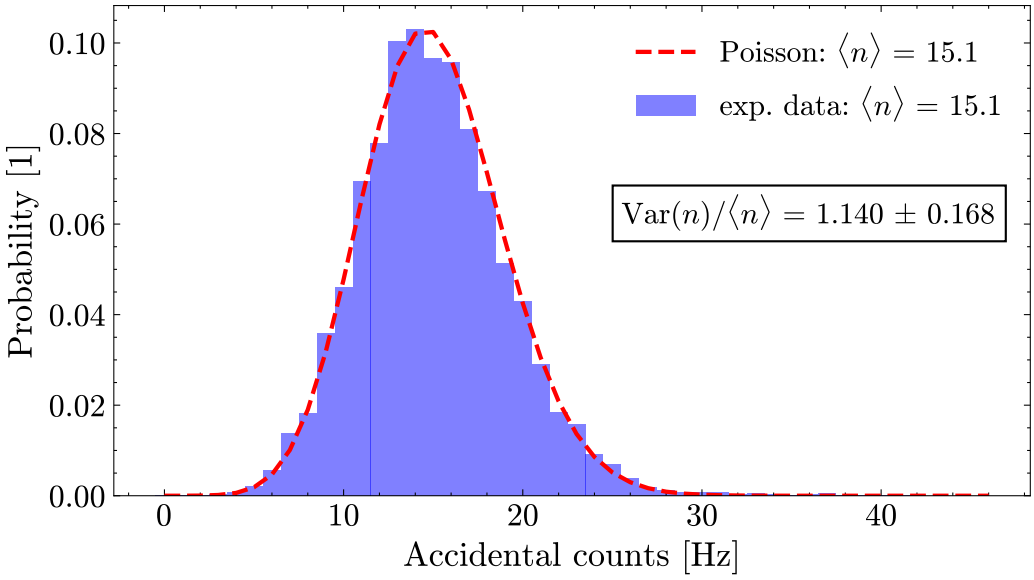

Figure 10.: Photon statistics of accidental counts

analysis were used, as well as the single counts in each arm, i.e., the exposure time is one second and the integration time is sixty seconds.

According to Equation 2.8, the accidental counts can be calculated at each time step using the single counts, coincidence counts and the coincidence window. This value is then compared with accidental counts measured experimentally. Again, in each time step, 105 values for the accidental counts were retrieved. In Figure 11, the theoretical values are compared with the experimental ones, where for the experimental counts the average and standard deviation is shown.

As can be seen, the theoretical values always fall within the standard deviation of the experimental ones. However, it is more important to consider whether the average value of the experimentally obtained counts can be well approximated by the formula, and thus, the theoretical values. This is decisive as the theoretical value obtained from Equation 2.8 is the estimator of the accidental counts in the transmittance model.

To determine the deviation between the theoretical value and the average of the experimental accidental counts, the relative error was calculated at each time step as follows:

$$\epsilon_{\mathrm{err}} = \frac{R_{\mathrm{acc}}^{\mathrm{theo}} - R_{\mathrm{acc}}^{\mathrm{exp}}}{R_{\mathrm{acc}}^{\mathrm{exp}}} \tag{4.1}$$

In the black box in Figure 11, the mean value and standard deviation of the relative error for the sixty time steps is shown. As can be seen, the average relative error between the two values is 1.6 %, so the formula can be used as a good approximation given the experimental uncertainties.

As a consequence, all parameters that are important for the transmittance model showed

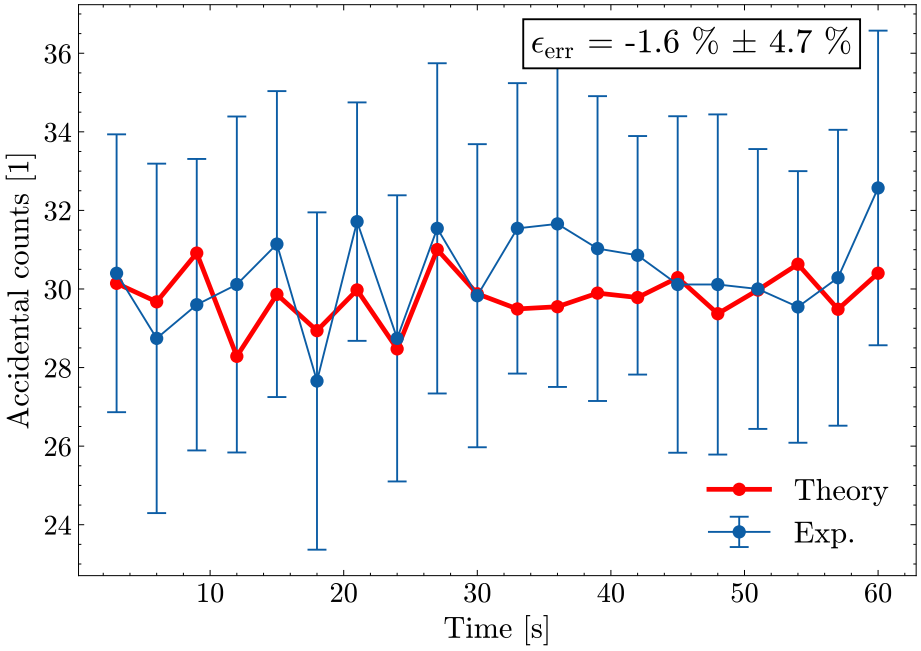

Figure 11.: Comparison between theoretically and experimentally obtained accidental counts

close agreement with the theoretical assumptions. As a next step, the approved model can be used to determine conditions in which the coincidence approach offers an advantage compared to the conventional one.

4.6. Heralding efficiencies

Before applying the experimental results in the simulation, two more important parameters for the theoretical model need to be determined, which are the heralding efficiencies of each arm.

They can be defined as the probability of detecting a photon in one arm given that a detection event has occurred in the other arm. For example, the heralding efficiency of the signal arm η_{sig}, conditioned on an idler detection, can be calculated using equations 2.2, 2.7 and 2.9:

$$\eta_{\text{sig}} = \frac{N_{\text{tot,cc}} - N_{\text{ac}}}{N_{\text{tot,idl}} - N_{\text{noise}}} = \frac{\eta_{\text{sig}}\eta_{\text{idl}}N_{\text{g}}}{\eta_{\text{idl}}N_{\text{g}}} \tag{4.2}$$

Analogously, the heralding efficiency of the idler arm η_{idl}, conditioned on the signal detection, is given by:

$$\eta_{\text{idl}} = \frac{N_{\text{tot,cc}} - N_{\text{ac}}}{N_{\text{tot,sig}} - N_{\text{noise}}} = \frac{\eta_{\text{sig}}\eta_{\text{idl}}N_{\text{g}}}{\eta_{\text{sig}}N_{\text{g}}} \tag{4.3}$$

It should be noted that the efficiency of the signal arm remains unchanged when a sample is placed in the idler arm. However, the efficiency of the idler arm itself decreases by a factor of T, the transmittance.

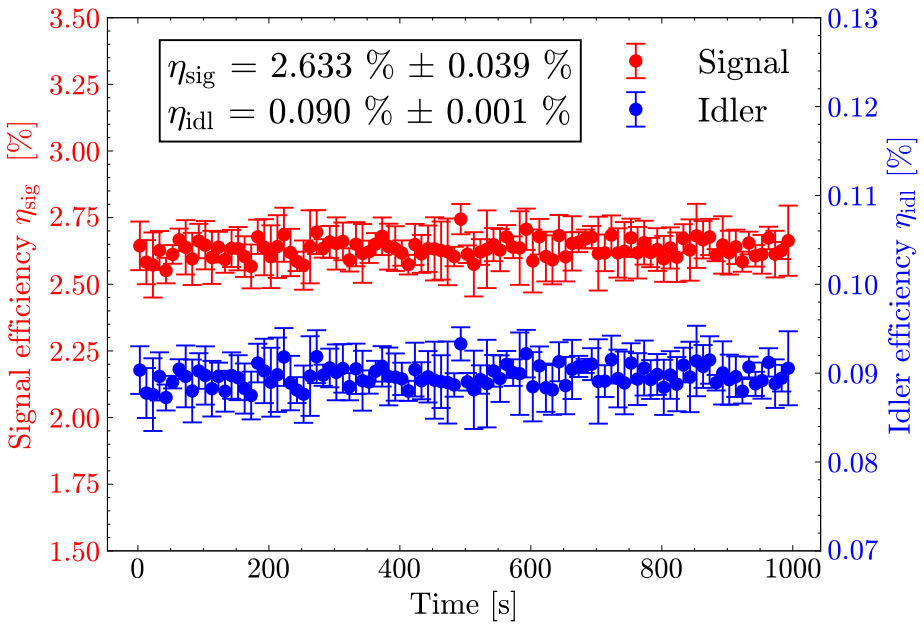

Figure 12.: Heralding efficiencies of the signal and idler arm

Both heralding efficiencies are crucial to assess the quality of the experimental setup, as they provide direct information about optical loss in each arm. Efficiencies are also important when setting up the transmittance model, as they are crucial for analytically calculating coincidence and accidental counts.
Representative values for the efficiencies were measured experimentally in the setup as they will be used in the analytical formulas. The exposure time was set to one second and the integration time to one thousand seconds. At each time step, the single counts and histogram were retrieved, and the efficiencies were calculated using equations 4.2 and 4.3. The measurement was repeated six times to obtain a statistical distribution of the efficiencies. The results are shown in Figure 12.
As can be seen, the efficiency of the idler arm is much smaller than that of the signal arm, at 0.09% and 2.63% respectively. The reasons for this difference may be the alignment of both arms and the different efficiencies of the single-photon detectors. The average value of the efficiencies and their standard deviation is displayed in the black box. As can be seen, the fluctuations of both values are quite small.
These two experimentally obtained efficiencies are used in the transmittance model to compare the conventional and coincidence approach in a simulation.

5. Simulation

The objective of the simulation model is to predict the conditions under which the coincidence approach achieves greater accuracy of the transmittance than the conventional ap-

Parameter	$R_{\text{noise,idl}}$**-sweep**	η_{sig}**-sweep**	R_{idl}**-sweep**
η_{idl} (%)	0.09	0.09	0.09
η_{sig} (%)	2.6	0 - 25	2.6
R_{idl} (kHz)	10	10	3 - 100
$R_{\text{noise,idl}}$ (kHz)	10 - 1000	1000	1000
$R_{\text{noise,sig}}$ (Hz)	7	7	7
T (1)	0.9	0.9	0.9

Table 2.: Overview of the simulation parameters for the different analysis scenarios

proach. The analytical formulas for calculating the variance of both approaches were given in Equation 2.12 and 2.6. The experiments showed that both coincidences and accidentals follow Poisson distribution, hence their variance in Equation 2.12 can be approximated by the mean value. However, in the conventional approach of Equation 2.6, the variance of the noise is approximated by the mean multiplied by a factor of 1.8, as determined by dark count measurements. Due to super-Poissonian distribution, the variance of the total single counts is approximated by the mean value multiplied by a factor of 2.2. This factor results from single-photon statistics in the idler arm, which were measured experimentally. For the following analysis, it is also assumed that the presence of the sample does not change the dark counts of the detectors.
There are six free parameters that need to be set in order to determine any values for both formulas:

- η_{idl}: efficiency of the idler arm
- η_{sig}: efficiency of the signal arm
- R_{idl}: photon rate in the idler arm
- $R_{\text{noise,idl}}$: noise rate in the idler arm
- $R_{\text{noise,sig}}$: noise rate in the signal arm
- T: transmittance of the sample

The idea of the simulation model is to select one of the six parameters and perform a sweep over a specified range to observe its impact on the variance of the transmittance in both approaches. The following analysis is not about investigating the influence of all six parameters, but is restricted to the efficiency of the signal arm, the ratio of the noise rate to the photon rate in the idler arm and the photon rate in the idler arm. To determine the effect of the noise-to-signal ratio on the variance of the transmittance, the noise rate in the idler arm was varied between zero and one hundred times the photon rate. An overview of all six parameters is shown in Table 2. The sample was chosen as a bandpass filter with a transmittance of $T = 0.9$ at 1400 nm [24].
The results of sweeping the noise rate in the idler arm are shown in Figure 13. As can

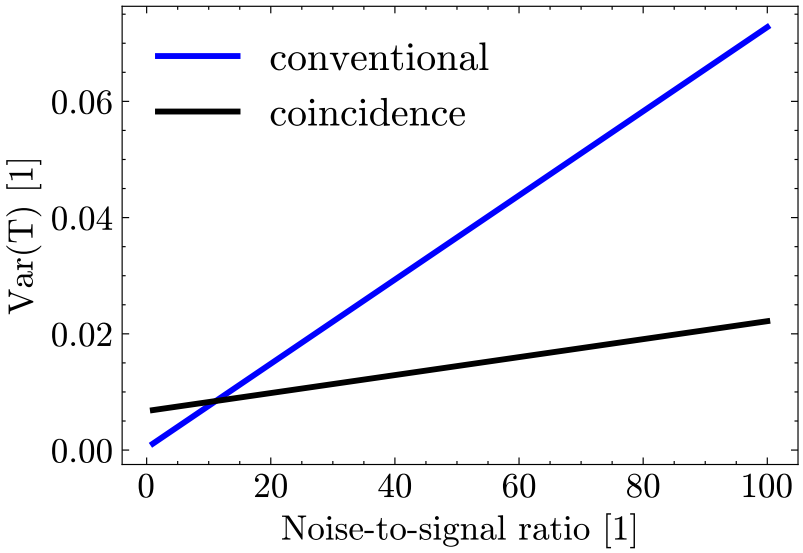

Figure 13.: Variance of the transmittance as a function of the noise-to-signal ratio

be seen, for noise-to-signal ratios smaller than eleven, the conventional approach results in smaller variance for transmittance. However, as the noise increases, the variance increases for both approaches, and the coincidence approach's slope is smaller than the conventional ones. Consequently, for noise-to-signal ratios greater than eleven, the coincidence approach shows smaller variance. One reason for this behavior may be that using a second arm with its imperfect efficiency lowers the overall accuracy when the noise rate is low. However, if the noise-to-signal ratio increases, the conventional approach becomes less precise because it cannot distinguish between photons that originate from a pair or from background counts??. Therefore, in a scenario with a high noise-to-signal ratio, the coincidence approach offers an advantage in terms of transmittance accuracy because it can distinguish between real photon pairs and noise.

In the second analysis, the efficiency of the signal arm is varied from zero to 25 percent. The values of the other parameters are listed in Table 2. As can be seen from the results in Figure 14, for a signal efficiency lower than one percent, the conventional approach results in lower variance than the coincidence approach. One reason for this may be that, with low signal efficiency, many coincidence counts remain undetected, resulting in lower transmittance accuracy. As the signal efficiency increases, the variance of the transmittance decreases for the coincidence approach because it depends quadratically on the reciprocal of the efficiency??. For the conventional approach, the variance of the transmittance remains constant because the signal arm does not have influence on the variance or measurement. Therefore, if the signal arm efficiency is greater than one percent, the coincidence approach is expected to provide more precise results than the conventional approach.

In the third analysis, the rate of detected photons in the idler arm was varied between three and one hundred kilohertz. The values of the other five parameters are shown in Table 2

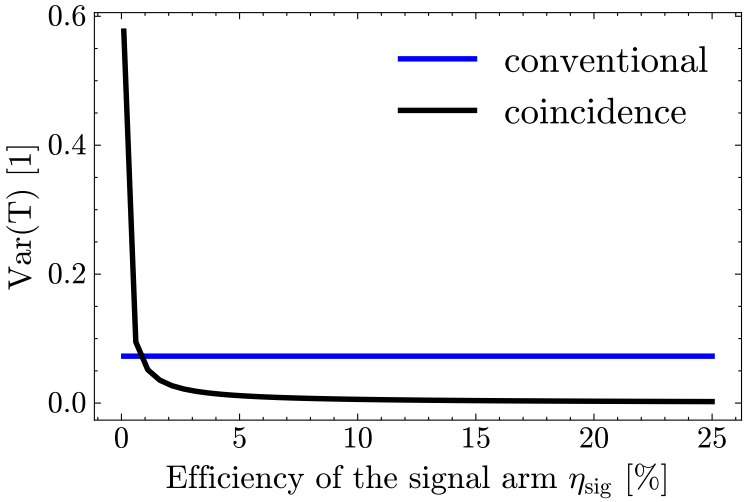

Figure 14.: Variance of the transmittance as a function of the efficiency in the signal arm

and the results of the analysis are displayed in Figure 15. It can be seen that for photon rates lower than twenty kilohertz the coincidence approach shows a smaller variance of the transmittance compared to the conventional approach, while for higher count rates both show similar results. One reason for this may be that at low photon rates the noise rate of one megahertz is comparably high and hence the conventional method cannot distinguish photons originating from a pair and dark counts. Therefore, the coincidence approach offers an advantage in terms of precision of the transmittance. With increasing count rate the difference between both methods becomes smaller as the influence of the noise rate decreases.

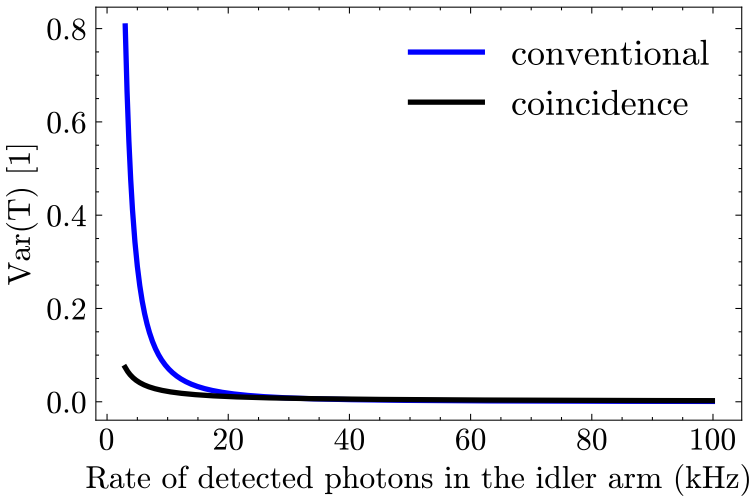

Figure 15.: Variance of the transmittance as a function of the photon rate in the idler arm

6. Conclusion

This work has investigated the precision of the transmittance estimation using temporally correlated photon pairs generated via spontaneous parametric down-conversion (SPDC) and compared it to a conventional single-photon approach. The central objective was to determine whether the coincidence-based detection scheme maintains an advantage in regimes dominated by noise.

To obtain a quantitative model of each method's precision, analytical expressions for the variance of the transmittance were derived through error propagation. This allows one to predict the precision of a given experimental setup in advance, without having to conduct multiple measurements to determine the variance of the desired parameter. To ensure that the model reflects realistic conditions, the photon statistics were investigated experimentally.

The experimental results revealed that single-photon statistics in both the idler and signal arms follow a mmBE distribution, confirming their super-Poissonian character. In contrast, coincidence and accidental counts exhibited Poissonian statistics, validating the theoretical assumption. Based on the experimental results and the analytical expressions for the variance of the transmittance, a numerical simulation model was created.

The simulation analyses investigated the dependence of the transmittance variance on key experimental parameters such as the signal arm efficiency, photon rate, and noise-to-signal ratio. The results showed that in noise-dominated regimes, i.e. when the noise-to-signal ratio is considerably large, the coincidence approach yields a lower variance and thus a higher precision than the conventional method. This advantage arises from the ability of coincidence detection to discriminate true photon-pair events from uncorrelated background noise. Additionally, the analysis demonstrated that the coincidence approach becomes more favorable with increasing signal arm efficiency, while at high photon rates and low noise levels both methods perform comparably.

Overall, the simulation confirms that coincidence-based detection of correlated photon pairs provides an advantage in precision under noisy conditions. The presented model predicts several parameter regions in which this advantage becomes significant.

Consequently, the next step is to verify the simulation results in an experimental setup to ascertain whether the coincidence approach delivers more precise results. In particular, it needs to be determined how to obtain variance experimentally. This can be achieved by repeating the measurement several times to obtain the statistical distribution, or by using linear error propagation.

Furthermore, it can be demonstrated to what extent the variance of the transmittance can be measured experimentally, and whether it is possible to measure up to the second decimal place. The maximum achievable precision in the experiment also limits the applicable parameter ranges in the simulation to determine the conditions under which the coincidence approach offers advantages in terms of precision.

Another aspect to consider is that, in regimes with a high noise-to-signal ratio, it may be difficult to distinguish accidental and coincidental counts in the histogram for low exposure times. The experiment must show whether increasing exposure time increases the difference between the two.

Appendix A.

Supplemental Information

Histogram

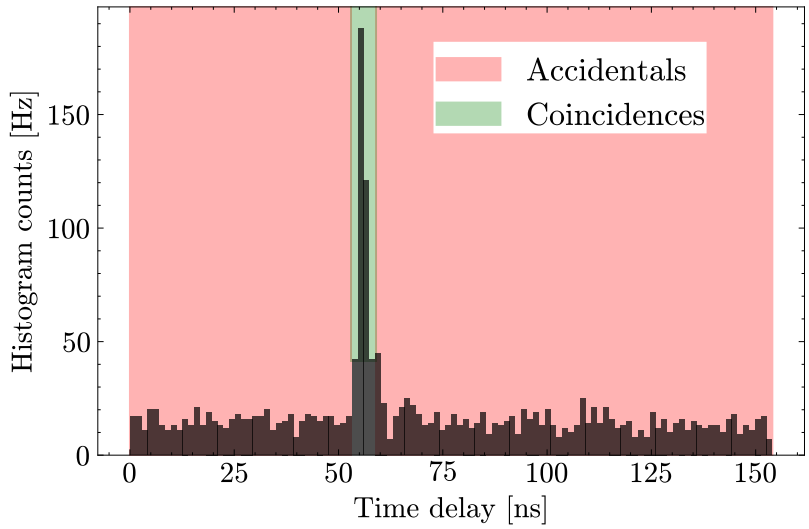

Figure A.1.: Representative coincidence histogram using the experimental setup

Afterpulsing

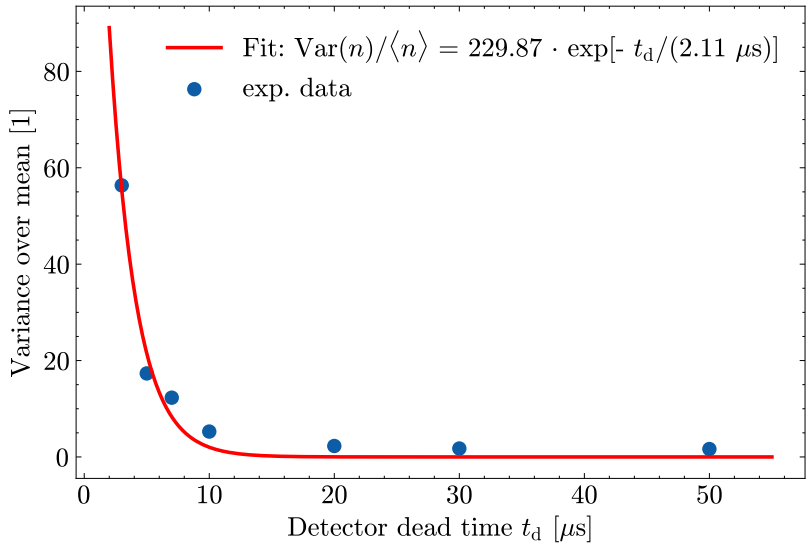

Figure A.2.: Variance-to-mean ratio as a function of the dead time of the IR single-photon detector

Dark counts SNSPD

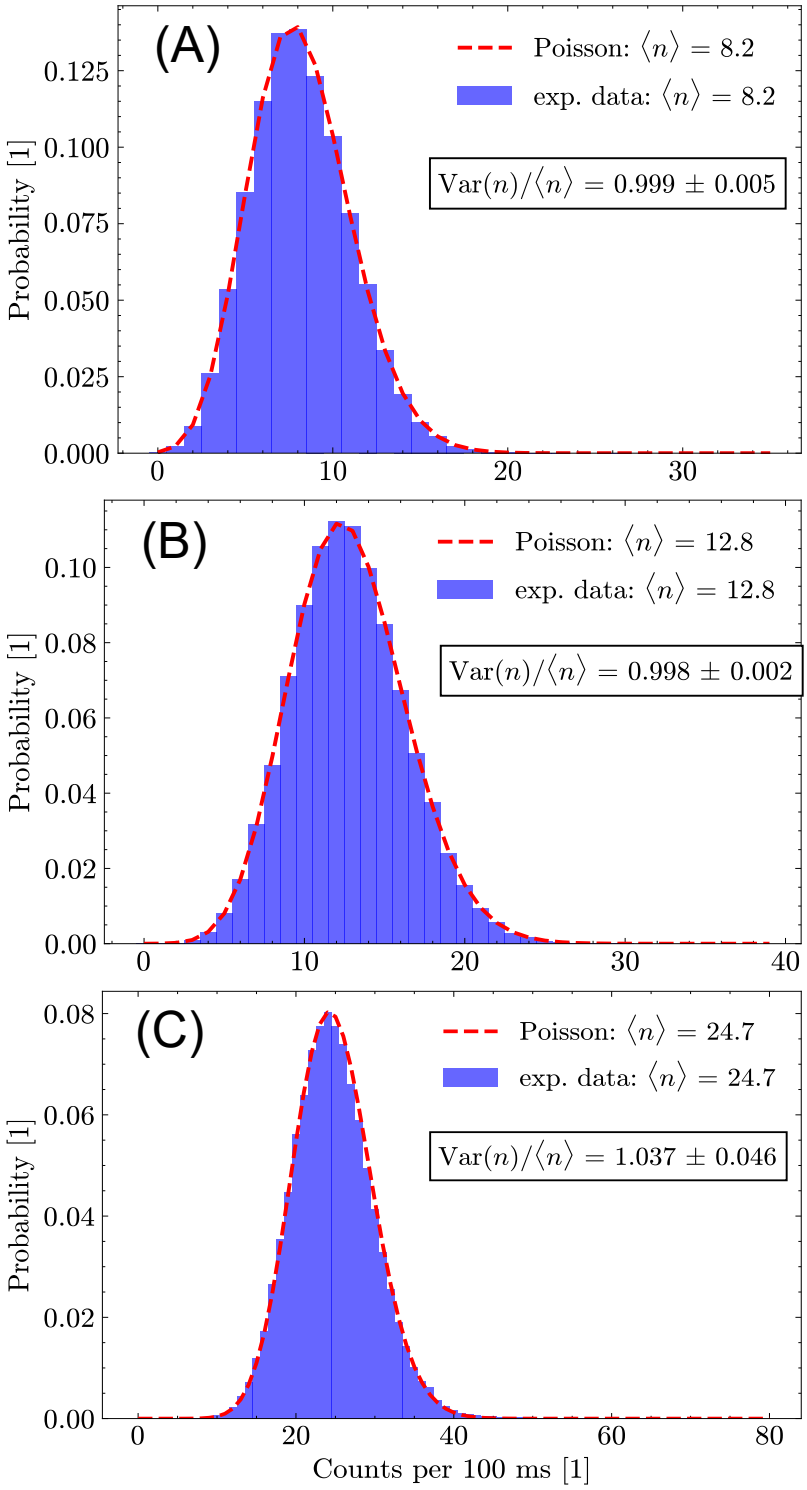

Figure A.3.: (A): Dark counts in SNSPD channel 2; (B): Dark counts in SNSPD channel 3; (C): Dark counts in SNSPD channel 4

Bibliography

[1] M. Avenhaus et al. “Photon Number Statistics of Multimode Parametric Down-Conversion”. In: *Physical Review Letters* 101.5 (Aug. 2008), p. 053601. ISSN: 0031-9007, 1079-7114. DOI: 10.1103/PhysRevLett.101.053601. (Visited on 08/28/2025).

[2] Robert W. Boyd. *Nonlinear Optics*. 3rd ed. Burlington, MA: Academic Press, 2008. ISBN: 978-0-12-369470-6.

[3] Hugo Defienne et al. “Advances in Quantum Imaging”. In: *Nature Photonics* 18.10 (Oct. 2024), pp. 1024–1036. ISSN: 1749-4885, 1749-4893. DOI: 10.1038/s41566-024-01516-w. arXiv: 2411.08415 [quant-ph]. (Visited on 08/28/2025).

[4] Marco Fiorentino et al. “Spontaneous Parametric Down-Conversion in Periodically Poled KTP Waveguides and Bulk Crystals”. In: *Optics Express* 15.12 (June 2007), pp. 7479–7488. ISSN: 1094-4087. DOI: 10.1364/OE.15.007479. (Visited on 09/03/2025).

[5] Daniel G. Fouche. “Detection and False-Alarm Probabilities for Laser Radars That Use Geiger-mode Detectors”. In: *Applied Optics* 42.27 (Sept. 2003), pp. 5388–5398. ISSN: 2155-3165. DOI: 10.1364/AO.42.005388. (Visited on 10/16/2025).

[6] Mark Fox. *Quantum Optics: An Introduction*. Oxford Master Series in Physics 15. Oxford ; New York: Oxford University Press, 2006. ISBN: 978-0-19-856672-4 978-0-19-856673-1.

[7] Marta Gilaberte Basset et al. “Perspectives for Applications of Quantum Imaging”. In: *Laser & Photonics Reviews* 13.10 (2019), p. 1900097. ISSN: 1863-8899. DOI: 10.1002/lpor.201900097. (Visited on 09/03/2025).

[8] Majeed M. Hayat, Sergio N. Torres, and Leno M. Pedrotti. “Theory of Photon Coincidence Statistics in Photon-Correlated Beams”. In: *Optics Communications* 169.1 (Oct. 1999), pp. 275–287. ISSN: 0030-4018. DOI: 10.1016/S0030-4018(99)00384-3. (Visited on 09/05/2025).

[9] Gerhard Humer et al. “A Simple and Robust Method for Estimating Afterpulsing in Single Photon Detectors”. In: *Journal of Lightwave Technology* 33.14 (July 2015), pp. 3098–3107. ISSN: 1558-2213. DOI: 10.1109/JLT.2015.2428053. (Visited on 10/16/2025).

[10] Genki Ishigane et al. “Label-Free Mid-Infrared Photothermal Live-Cell Imaging beyond Video Rate”. In: *Light: Science & Applications* 12.1 (July 2023), p. 174. ISSN: 2047-7538. DOI: 10.1038/s41377-023-01214-2. (Visited on 09/10/2025).

[11] Ryo Kato et al. “Label-Free Visualization of Photosynthetic Microbial Biofilms Using Mid-Infrared Photothermal and Autofluorescence Imaging”. In: *Analyst* 148.24 (Dec. 2023), pp. 6241–6247. ISSN: 1364-5528. DOI: 10.1039/D3AN01453C. (Visited on 09/10/2025).

[12] Jin-Woo Kim et al. “Photon-Counting Statistics-Based Support Vector Machine with Multi-Mode Photon Illumination for Quantum Imaging”. In: *Scientific Reports* 12.1 (Oct. 2022), p. 16594. ISSN: 2045-2322. DOI: 10.1038/s41598-022-20501-3. (Visited on 09/09/2025).

[13] H.H. Ku. “Notes on the Use of Propagation of Error Formulas”. In: *Journal of Research of the National Bureau of Standards, Section C: Engineering and Instrumentation* 70C.4 (Oct. 1966), p. 263. ISSN: 0022-4316. DOI: 10.6028/jres.070C.025. (Visited on 09/05/2025).

[14] Paul G. Kwiat et al. “Ultrabright Source of Polarization-Entangled Photons”. In: *Physical Review A* 60.2 (Aug. 1999), R773–R776. DOI: 10.1103/PhysRevA.60.R773. (Visited on 09/03/2025).

[15] Yuanfan Lai et al. “The Impact of Afterpulsing Effects in Single-Photon Detectors on the Performance Metrics of Single-Photon Detection Systems”. In: *Photonics* 11.11 (Nov. 2024), p. 1074. ISSN: 2304-6732. DOI: 10.3390/photonics11111074. (Visited on 10/16/2025).

[16] Gabriela Barreto Lemos et al. “Quantum Imaging with Undetected Photons”. In: *Nature* 512.7515 (Aug. 2014), pp. 409–412. ISSN: 1476-4687. DOI: 10.1038/nature13586. (Visited on 09/10/2025).

[17] Leonard Mandel and Emil Wolf. *Optical Coherence and Quantum Optics*. Cambridge: Cambridge University Press, 1995. ISBN: 978-0-521-41711-2. DOI: 10.1017/CBO9781139644105. (Visited on 09/09/2025).

[18] Paul-Antoine Moreau et al. “Imaging with Quantum States of Light”. In: *Nature Reviews Physics* 1.6 (May 2019), pp. 367–380. ISSN: 2522-5820. DOI: 10.1038/s42254-019-0056-0. (Visited on 08/28/2025).

[19] J. Sabines-Chesterking et al. “Sub-Shot-Noise Transmission Measurement Enabled by Active Feed-Forward of Heralded Single Photons”. In: *Physical Review Applied* 8.1 (July 2017), p. 014016. DOI: 10.1103/PhysRevApplied.8.014016. (Visited on 10/15/2025).

[20] J. Sabines-Chesterking et al. “Twin-Beam Sub-Shot-Noise Raster-Scanning Microscope”. In: *Optics Express* 27.21 (Oct. 2019), pp. 30810–30818. ISSN: 1094-4087. DOI: 10.1364/OE.27.030810. (Visited on 10/15/2025).

[21] James Schneeloch et al. “Introduction to the Absolute Brightness and Number Statistics in Spontaneous Parametric Down-Conversion”. In: *Journal of Optics* 21.4 (Feb. 2019), p. 043501. ISSN: 2040-8986. DOI: 10.1088/2040-8986/ab05a8. (Visited on 09/09/2025).

[22] *Single Quantum - Excellence in Photon Detection*. https://www.singlequantum.com/. (Visited on 10/14/2025).

[23] S. Tanzilli et al. *Highly Efficient Photon-Pair Source Using a Periodically Poled Lithium Niobate Waveguide*. Dec. 2000. DOI: 10.48550/arXiv.quant-ph/0012053. arXiv: quant-ph/0012053. (Visited on 09/03/2025).

[24] *Thorlabs - FBH1400-12 Hard-Coated Bandpass Filter, Ø25 mm, CWL = 1400 nm, FWHM = 12 nm*. https://www.thorlabs.com. (Visited on 10/22/2025).